



HAL
open science

Experiments and DFT Computations Combine to Decipher Fe-Catalyzed Amidine Synthesis through Nitrene Transfer and Nitrile Insertion

Guillaume Coin, Patrick Dubourdeaux, Frédéric Avenier, Ranjan Patra, Ludovic Castro, Colette Lebrun, Pierre-Alain Bayle, Jacques Pécaut, Geneviève Blondin, Pascale Maldivi, et al.

► **To cite this version:**

Guillaume Coin, Patrick Dubourdeaux, Frédéric Avenier, Ranjan Patra, Ludovic Castro, et al.. Experiments and DFT Computations Combine to Decipher Fe-Catalyzed Amidine Synthesis through Nitrene Transfer and Nitrile Insertion. *ACS Catalysis*, 2021, 11 (4), pp.2253-2266. 10.1021/acscatal.0c03791 . hal-03176777

HAL Id: hal-03176777

<https://hal.science/hal-03176777>

Submitted on 18 Nov 2021

HAL is a multi-disciplinary open access archive for the deposit and dissemination of scientific research documents, whether they are published or not. The documents may come from teaching and research institutions in France or abroad, or from public or private research centers.

L'archive ouverte pluridisciplinaire **HAL**, est destinée au dépôt et à la diffusion de documents scientifiques de niveau recherche, publiés ou non, émanant des établissements d'enseignement et de recherche français ou étrangers, des laboratoires publics ou privés.

Experiments and DFT computations combine to decipher Fe-catalyzed amidine synthesis through nitrene transfer and nitrile insertion.

Guillaume Coin,^{#,&} Patrick Dubourdeaux,[#] Frédéric Avenier,[£] Ranjan Patra,^{#+} Ludovic Castro,[§] Colette Lebrun,[§] Pierre-Alain Bayle,[§] Jacques Pécaut,[§] Geneviève Blondin,[#] Pascale Maldivi^{§*} and Jean-Marc Latour^{#*}

[#] Univ. Grenoble Alpes, CEA, CNRS, IRIG, DIESE, LCBM, pmb, F-38000 Grenoble, France

[&] Univ. Grenoble Alpes, CNRS UMR 5250, DCM, CIRE, F-38000 Grenoble, France

[§] Univ. Grenoble Alpes, CEA, CNRS, IRIG, DIESE, SyMMES, F-38000 Grenoble, France

[§] Univ. Grenoble Alpes, CEA, IRIG, MEM, F-38000 Grenoble, France

[£] Univ. Paris Saclay, ICMO, CNRS, UMR 8182, F-91405 Orsay, France

⁺ Amity Institute of Click Chemistry Research & Studies (AICCRS), Amity University Noida 201303, India

KEYWORDS: *Amidine synthesis, multicomponent reaction, nitrene transfer, DFT calculations, mechanism*

Multicomponent reactions are attracting strong interest as they contribute to develop more efficient synthetic chemistry. Understanding their mechanism is thus an important issue to optimize their operation. However, it is also a challenging task owing to the complexity of the succession of molecular events involved. Computational methods have recently proven of utmost interest to help deciphering some of these processes and the development of integrated experimental and theoretical approaches thus appear as most powerful to understand these mechanisms at the molecular level. A good example is given by the synthesis of amidines which are important pharmaceutical compounds. Their synthesis requires the association of three components, often an alkyne, a secondary amine and an organic azide as nitrene precursor. We found that an alternative way is offered by an Fe-catalyzed combination of a hydrocarbon, a nitrile and a nitrene which gives amidines in good yields under mild conditions. The efficiency of the transformation and the paucity of mechanistic information on these reactions prompted us to thoroughly investigate its mechanism. Several mechanistic *scenarii* were explored using experimental techniques including radical trap and ¹⁵N labeling studies combined to DFT calculations of reaction profiles. This allowed us to show that the amidination reaction involves the trapping of an intermediate substrate cation by an Fe-released acetonitrile molecule pointing to a true multicomponent reaction occurring exclusively within the cage around the metal center. Moreover, the calculated energy barriers of the individual steps explained how amidination outweigh direct amination in these reactions. The perfect consistency between DFT results and specific experiments to validate them strongly support these mechanistic conclusions and highlights the potency of this combined approach.

INTRODUCTION

Functionalization of C - H bonds in "one-pot" processes is intensely sought-after because it allows several bond-forming steps without requiring intermediate purification procedures, thereby minimizing waste generation and saving time.¹ These processes can develop along different ways associating several reactions and have been coined domino, cascade or tandem reactions. Alternatively, several reagents can combine to give a product without formation of an intermediate product in a multicomponent reaction.² Quite understandably, the mechanisms of these reactions are hugely complex but their elucidation is highly desirable to optimize their efficacies and

selectivities. Fortunately, the past ten years have witnessed immense progresses in the development of computational methods which are now able to describe complicate mechanistic landscapes.³ Moreover, recent work has shown that intermingling them to experimental investigations is a very powerful approach.^{4,5} In the present work, we have used this approach to try to understand the mechanism of formation of amidines through a multicomponent reaction associating a hydrocarbon, a nitrile and an amine delivered as a nitrene.

Amidines bear a strong medicinal and pharmaceutical interest⁶ both for their intrinsic properties and their involvement in the syntheses of numerous heterocycles.^{7,8} As a matter of fact,

the amidine function allows to form strong ionic or H-bond interactions or to chelate transition metals which has led to its inclusion in many enzyme substrates or inhibitors.^{9,10} This strong interest motivates continuous efforts to design new synthetic routes to a large panel of amidine derivatives, especially sulfonyl-¹¹⁻¹⁴ and acyl-^{5,15} amidines. Amidine syntheses have been devised from many functional groups (amides and thioamides, isonitriles)¹⁶ but more generally amidines are accessible from condensation of primary amines with electron-deficient nitriles^{16,17} (or acetals).¹⁷ Whereas this can be achieved using high temperatures, catalysis by acidic metals affords amidines in milder conditions.¹⁸ Simultaneous binding of the two reagents to a (high-valent) metal facilitates the nucleophilic addition of the amine to the nitrile. Numerous examples of this stoichiometric reaction have been reported.^{18,19} In the past fifteen years, several metal-catalyzed multi-component reactions have been reported to produce amidines efficiently from a hydrocarbon, an amine and a nitrogen reagent which is often a nitrene precursor.^{5,11-13,15,20-24} As a typical example, when an alkyne was reacted with a secondary amine and an organic azide in presence of a Cu^I (or Ag^I) salt, a triazolyl copper species was proposed to be the key intermediate in the coupling of the nitrene to the alkyne after liberation of N₂.^{11-13,21} Very recently, a similar reaction was developed by Van Vliet *et al.* using as nitrene precursors 1,4,2-dioxazol-5-ones which liberate CO₂ when forming an acylnitrene, and the mechanism of the reaction was investigated by ³¹P NMR and DFT calculations.⁵

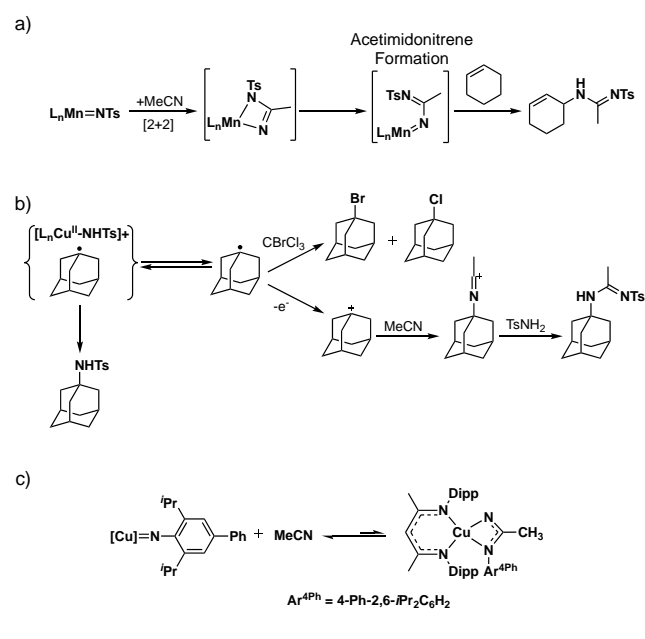
Intriguingly, nitriles were used scarcely in these multicomponent processes: reaction with phenyl diazonium produces the highly electrophilic nitrilium cation which can be trapped by a sulfonamide.²⁰ In this respect, it must be noted that the catalytic formation of amidines from nitriles by a totally different synthetic method has been reported in a limited number of cases. As a matter of fact, upon studying nitrene transfer catalysis by various metal complexes, Evans *et al.* noted that the reaction of cyclohexene with the iodine PhI=NTs in acetonitrile in the presence of Mn (or Fe) tetraphenylporphyrin afforded 3-tosylacetamidinocyclohexene in 63 % (with respect to PhI=NTs, Scheme 1a).²⁵ More recently, Bagchi *et al.* reported a similar insertion of acetonitrile in the final amination product in the Cu-catalyzed reaction of PhI=NTs with aliphatic substrates (adamantane, *cis*-1,4-dimethyl-cyclohexane, 2-methylbutane) leading to the corresponding amidines in yields ranging from 16 to 32 % (Scheme 1b).²⁶ These amidine syntheses are thus akin to a multicomponent reaction associating an olefin and a nitrile to an amine in the form of a nitrene.

There is no consensus on the mechanism of this acetonitrile insertion. Evans *et al.* hypothesized that the reaction involves the formation of a diazametallocyclobutane intermediate formed by condensation of acetonitrile with a tosylimido species (Scheme 1a).²⁵ An amidine-derived nitrene would thus be transferred to the substrate. This proposal was not supported by experimental observations. Such support was very recently provided by Bakhoda *et al.* in their study of copper aryl nitrene intermediates (Scheme 1c).²⁷ Actually, these authors were able to evidence an equilibrium between a copper imide and the related copper amidinate resulting from acetonitrile insertion. Support for the latter structure was brought by infrared spectroscopy with the help of a ¹³C labeling study. When the two species in equilibrium were treated by ethylbenzene, only the corresponding amine was formed. No acetamidine was formed by reaction either with PMe₃ or ^tBuNC. It must be

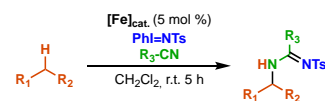
noted that the imide / acetamidinate equilibrium is significantly displaced toward the former (4:1), which may be one reason for the exclusive formation of the amine product. Bagchi *et al.* studied the mechanism of amidine formation catalyzed by their copper complex.²⁶ By using CBrCl₃ as radical trap, they were able to conclude that H[•] abstraction from adamantane by the copper imido active species led to the formation of the adamantyl radical which escaped in the solution (Scheme 1b). They proposed that the radical was then oxidized in solution to the adamantyl cation, the latter next reacting with acetonitrile to form the acetimino carbocation which was trapped by tosylamine present in the medium. Whereas the formation of the adamantyl radical was evidenced, its oxidation and further reactions were not supported either experimentally or computationally.

Scheme 1. Mechanistic proposals for amidine syntheses involving nitrene transfer reactions.

Previous mechanism proposal



This work

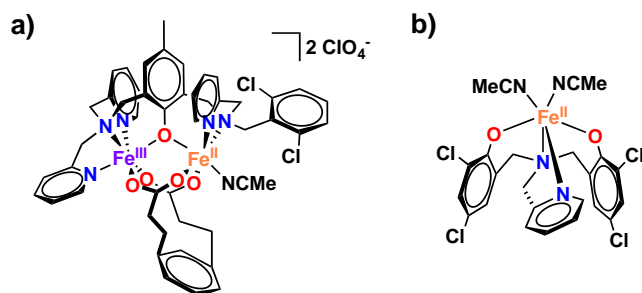


We reported recently that the diiron complex **[1.Fe^{II}(NCMe)]²⁺**,^{28,29} (Scheme 2a) exhibits a high efficiency in nitrene transfer catalysis using PhI=NTs as nitrene precursor.²⁹ Through ElectroSpray Ionization-Mass Spectrometry two active species were evidenced and are hereafter designated **[1.Fe^{IV}(NTs)]²⁺** and **[1.Fe^V(NTs)]²⁺**.^{30,31} DFT analyses of their electronic structure showed, in both cases, significant charge transfer from both ligands NTs and **1** to the high-valent Fe generating actual configurations involving ligand radicals such as **[1.Fe^{III}(NTs)]²⁺** and **[1.Fe^{IV}(NTs)]²⁺**, respectively. This complex is indeed an efficient catalyst for aziridination of styrenes (yields ca 80 %) and other olefins.^{32,33} A more moderate activity was noted for amination of ethylbenzenes (yields ca 50 %) in dichloromethane using PhI=NTs as nitrene precursor.³¹ By contrast, we found that running the reaction in ace-

tonitrile led to higher conversion and interestingly to the major formation of the corresponding acetamidines. Moreover, the acetamidine is the exclusive product formed in the same conditions when cyclohexane is used as substrate (Scheme 1d). This suggests that the amine vs amidine distribution is highly dependent on the hydrocarbon substrate, the amidine being favored for those having a higher bond dissociation energy (BDE), in line with a H[•] abstraction process being part of the mechanism. The fact that a high conversion to amidine can be achieved and that no mechanistic consensus exists for acetonitrile insertion in aliphatic amination product prompted us to study these processes in more details.

Our earlier studies of nitrene transfer catalyzed by $[1.\text{Fe}^{\text{II}}(\text{NCMe})]^{2+}$ revealed that its ferric site (Scheme 2a) did not change redox state during catalysis which involved activation of the Fe^{II} site formally to Fe^{IV} and Fe^V.^{30,31} This incited us to develop simpler monoiron catalysts with similar environments (Scheme 2b). We observed that the monoiron catalyst $[2.\text{Fe}^{\text{II}}(\text{NCMe})_2]$ (Scheme 2b) exhibited a mechanistically similar reactivity for styrene aziridination albeit with more modest conversions.^{33,34} DFT analyses of the electronic structure of the purported active species $[2.\text{Fe}^{\text{IV}}(\text{NTs})]$ and of the reaction profile led to attribute this lower efficacy to a significantly smaller electron affinity of $[2.\text{Fe}^{\text{IV}}(\text{NTs})]$ vs $[1.\text{Fe}^{\text{IV}}(\text{NTs})]^{2+}$ and $[1.\text{Fe}^{\text{V}}(\text{NTs})]^{2+}$. Here also we observed that the mononuclear system led to similar reactivity as $[1.\text{Fe}^{\text{II}}(\text{NCMe})]^{2+}$ with major formation of amidine vs amine albeit in significantly lower amounts. This entitled us to perform a theoretical analysis of the electronic structures of the active species and the reaction pathways using the monoiron system. Indeed, the size combined to the complex spin state situation preclude the calculation of reaction pathways for the diiron system.

Scheme 2. Structure of the catalysts used in this study: a) $[1.\text{Fe}^{\text{II}}(\text{NCMe})]^{2+}$ and b) $[2.\text{Fe}^{\text{II}}(\text{NCMe})_2]$



Initial exploration of the dependence of amine vs amidine formation from ethylbenzene on acetonitrile concentration revealed two distinct regimes. At low MeCN concentration, a saturation phenomenon was observed where amine formation was suppressed by acetonitrile concentration increase, pointing to binding of MeCN to the catalyst. At saturation, the amidine / amine ratio reached a constant value which suggested the trapping by MeCN of a common intermediate. DFT calculations of the reaction profiles for ethylbenzene highlighted that, after H[•] abstraction and electron transfers, attack of substrate radical or cation by Fe-released acetonitrile emerged as the more likely mechanism to form amidine. This molecular mechanism was supported by radical trap and ¹⁵N-labeling specific experiments. Moreover, DFT calculations of the reaction profiles for cyclohexane allow us to propose an overall

mechanism explaining the competitive formations of amine and amidine from ethylbenzene and the exclusive formation of amidine for cyclohexane. This overall reaction scheme was further strengthened using a kinetic model involving competitive reaction rates.

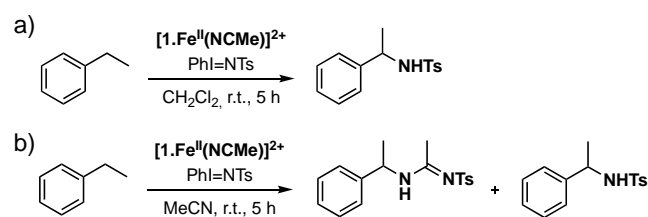
RESULTS

Catalytic acetamidine formation during amination of hydrocarbons in acetonitrile

(i) General features of the reaction.

We reported recently that the diiron system $[1.\text{Fe}^{\text{II}}(\text{NCMe})]^{2+}$ catalyzes the amination of ethylbenzene by PhI=NTs with a yield of 54 % using molar ratios catalyst/PhI=NTs/ethylbenzene 0.05/1/50 in dichloromethane at room temperature for 5 h (Scheme 3a).³¹ Changing the solvent to acetonitrile in identical conditions afforded conversion to a mixture of the amine and the corresponding acetamidine in the ratio 1:~6 (Scheme 3b and Table 1).

Scheme 3. Catalysis of nitrene transfer to ethylbenzene



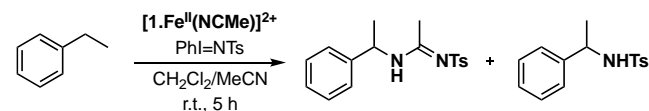
The two products have been identified by ESI-MS and by their ¹H-NMR signatures and they were quantitated easily together with tosylamine in the crude reaction mixture. It is noteworthy that the catalytic solution is red in color and has a maximum absorption in the visible region at 482 nm (Figure S1). This observation indicates that the species active in the catalysis of amidine formation is formally the $[\text{Fe}^{\text{III}}\text{Fe}^{\text{V}}(=\text{NTs})]$ complex ($[1.\text{Fe}^{\text{V}}(\text{NTs})]^{2+}$).³¹ In the same conditions, the use of $[2.\text{Fe}^{\text{II}}(\text{NCMe})_2]^{2+}$ as catalyst affords only a small amount of acetamidine (4 %) together with trace amounts of amine, which is consistent with its diminished nitrene transfer efficacy.

(ii) Influence of acetonitrile content on amidine formation

We then investigated the influence of acetonitrile content on amidine formation by varying the composition of the reaction solvent dichloromethane/acetonitrile from 100/0 to 0/100 v/v. Figure 1 illustrates the variation of the ratio $Y = \text{yield}_{\text{amidine}} / (\text{yield}_{\text{amine}} + \text{yield}_{\text{amidine}})$ as a function of the number (N) of equivalents of acetonitrile with respect to ethylbenzene (EB). In the conditions used (catalyst/PhI=NTs/ethylbenzene 0.05/1/50), N varies from 0 in dichloromethane to ca 11 in acetonitrile. We observed that Y varies from 0 to 0.86 (86 % acetamidine) with a plateau that is reached at ca N=1.2 corresponding to a proportion of 10 % v/v acetonitrile in dichloromethane. Therefore, two regimes can be distinguished. (i) At low acetonitrile/ethylbenzene ratio $N \leq 1.2$ (Figure 1, inset), the curvature of the data observed when increasing the acetonitrile

content is reminiscent of Michaelis-Menten behavior³⁵ (see SI Thermodynamic and kinetic modeling section) and clearly indicative of a saturation behavior and the occurrence of a binding equilibrium. This suggests that binding of acetonitrile to $[1.\text{Fe}^{\text{V}}(\text{NTs})]^{2+}$ is involved in acetamide formation. (ii) At high acetonitrile/ethylbenzene ratio $N \geq 1.2$, however, full acetamide formation is not reached since Y plateaus at 0.86. This indicates that nitrile transfer to form amine can never be totally outweighed by

Table 1. Catalysis of ethylbenzene amidination by $\text{PhI}=\text{NTs}$ in dichloromethane/acetonitrile mixtures^a



Entry	Nitrile (% v/v)	N ^b	Y ^c (%)
1	0	0	0
2	2.5	0.27	57
3	5	0.54	71
4	7.5	0.81	79
5	10	1.08	79
6	25	2.69	86
7	50	5.38	86
8	100	10.8	86

^a Conditions $[1.\text{Fe}^{\text{II}}(\text{NCMe})]^{2+}/\text{PhI}=\text{NTs}/\text{EB} = 0.05/1/50$, 25 °C, 5 h;

^b N: number of molar equivalents of acetonitrile vs EB;

^c $Y = (\text{yield}_{\text{amidine}}) / [(\text{yield}_{\text{amidine}}) + (\text{yield}_{\text{amine}})]$

amidine formation, pointing to a competition between the two that does not depend on acetonitrile concentration. To get more insights into this mechanism, we investigated the steric and electronic influences of the nitrile.

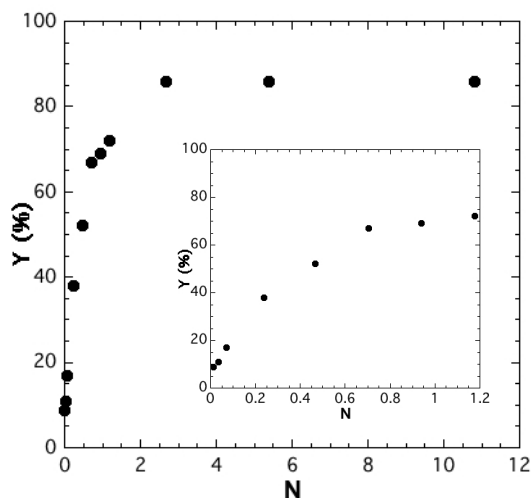
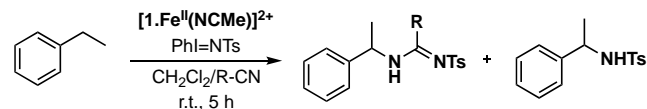


Figure 1. Variation of the amidine formation ratio Y with the acetonitrile content from pure dichloromethane ($N = 0$) to pure acetonitrile ($N = 10.78$). Inset: expansion of the domain $0 < N < 1.2$.

(iii) Influence of nitrile nature on amidine formation

To evaluate the influence of the steric properties of the nitrile on amidine formation, we compared the yields of amidine in the series $\text{R}-\text{C}\equiv\text{N}$ with $\text{R} = \text{Me}, \text{Et}, n\text{-Pr}, n\text{-Bu}$ and $t\text{-Bu}$ (Table 2, entries 1-5). The reactions were performed at a ratio catalyst/ $\text{PhI}=\text{NTs}/\text{EB}/\text{nitrile} = 0.05/1/50/15$. We chose to use a small number of equivalents of nitrile vs EB ($N = 0.3$) to maximize its potential effect (Figure 1) which would possibly be masked by working in conditions of the plateau ($N > 1.2$). ¹H-NMR analyses of the reaction mixtures revealed an almost constant proportion of amidine $45 \pm 4\%$ in the reaction mixture. These observations indicate that neither the small variation of electronic influence of the alkyl groups nor their strongly increasing bulkiness have any notable influence on the product distribution. The irrelevance of nitrile bulkiness suggests that it binds to the Fe ion through its nitrogen, therefore pushing the R group away from the reaction site. By contrast, in these conditions, benzonitrile gave a drastically reduced amidine proportion of 22 % (Table 2, entry 6). To investigate the latter point further, we compared the series with $\text{R} = \text{Me}, \text{Ph}$ and $p\text{-CF}_3\text{Ph}$ in the conditions catalyst/ $\text{PhI}=\text{NTs}/\text{ethylbenzene}/\text{nitrile} = 0.05/1/50/25$ ($N = 0.5$) which allow a higher conversion to the amidine (Table 2, entries 7-9). Consistently, the respective yields of amidine were 70 % for $\text{R} = \text{Me}$, 61 % for $\text{R} = \text{Ph}$ and 32 % for $\text{R} = p\text{-CF}_3\text{Ph}$. These results support that the more electron-rich nitriles give a higher conversion to amidine.

Table 2. Influence of nitrile on amidine vs amine distribution^a



Entry	R (R-C≡N)	Y ^c	Conv. ^d
1	Me	49	52
2	Et	49	42
3	Pr	41	40
4	ⁿ Bn	47	41
5	^t Bu	45	47
6	Ph	22	39
7 ^b	Me	70	55
8 ^b	Ph	61	49
9 ^b	(<i>p</i> -CF ₃)Ph	32	46

^a Entries 1-6 conditions $[1.\text{Fe}^{\text{II}}(\text{NCMe})]^{2+}/\text{PhI}=\text{NTs}/\text{EB}/\text{nitrile} = 0.05/1/50/15$, 25 °C, 5 h;

^b Entries 7-9 conditions $[1.\text{Fe}^{\text{II}}(\text{NCMe})]^{2+}/\text{PhI}=\text{NTs}/\text{EB}/\text{nitrile} = 0.05/1/50/25$, 25 °C, 5 h;

^c $Y = (\text{yield}_{\text{amidine}}) / [(\text{yield}_{\text{amidine}}) + (\text{yield}_{\text{amine}})]$ in %

^d Conversion vs $\text{PhI}=\text{NTs}$ in %

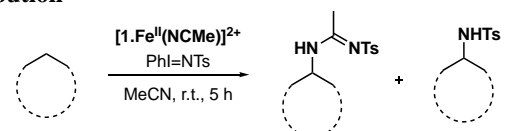
(iv) Influence of the hydrocarbon substrate on amidine formation

As mentioned above, when cyclohexane was used in similar conditions, the reaction produced only acetamide in 22 % yield (Table 3). The fact that no amine was formed, whereas it is always produced in ethylbenzene amination, suggests that

the H[•] abstraction difficulty may play a significant role in the amine/amidine distribution.

We thus studied the transformation of various substrates, the BDE of which span the range from 85 kcal mol⁻¹ (EB) to 99 kcal mol⁻¹ (cyclohexane). As shown in Table 3, cyclooctane and cycloheptane which possess BDE values > 94 kcal mol⁻¹ again gave no amine. By contrast, indane which has a BDE close to that of ethylbenzene gave a strongly enhanced formation of amine (43 % vs 8 % for ethylbenzene). The small difference in BDE values (0.5 kcal mol⁻¹) cannot explain this difference, which can tentatively be related to the higher number of indane benzylic positions.

Table 3. Influence of substrate on amine vs amidine distribution^a



Substrate	BDE ^b	Conv. ^c	Amidine ^d	Amine ^d
Cyclohexane ^a	99	22	100	0
Cyclooctane ^a	96	24	100	0
Cycloheptane ^a	94	29	100	0
THF ^a	92	50	0	100
Indane ^c	85.9	44	57	43
Ethylbenzene ^a	85.4	74	92	8

^a Conditions $[1.Fe^{II}(NCMe)]^{2+}/PhI=NTs/substrate = 0.05/1/100$, acetonitrile, 25 °C, 5 h;

^b Bond Dissociation Energy in kcal mol⁻¹.³⁶

^c Conversion vs PhI=NTs in %.

^d Distribution of amidine and amine in %.

^e Conditions $[1.Fe^{II}(NCMe)]^{2+}/PhI=NTs/substrate = 0.05/1/50$, acetonitrile, 25 °C, 5 h.

We studied also the transformation of THF which has a BDE (92 kcal mol⁻¹) comparable to that of cycloheptane. Only the amine (2-tosylaminotetrahydrofuranne) was formed in 50 % yield and no amidine was detected (Table 3). This difference of reactivity between THF and cycloheptane most probably comes from the possibility of THF to bind the catalyst active species $[1.Fe^V(NTs)]^{2+}$: binding of THF would outcompete nitrile binding and thereby inhibit amidine formation.

(v) Summary of mechanistically relevant features

These experimental studies have unveiled a number of important features which any realistic mechanistic proposal must account for. (i) Acetamidine formation involves binding of acetonitrile to the catalyst in an equilibrium as evidenced by the dependency of Y on acetonitrile content. Binding of acetonitrile is also supported by THF inhibition of acetamidine formation. Lastly, amidine formation is favored for electron rich nitriles, which can bolster both nitrile binding to Fe and nucleophilic attack of the substrate. (ii) Amidine formation never suppresses amine formation in case of ethylbenzene, which suggests that a competition exists between the two reactions. Moreover, when the hydrocarbon BDE increases (as for cyclohexane), only amidine is formed which suggests that H[•] abstraction or radical rebound is in competition with acetonitrile binding or a subsequent process. (iii) UV-visible monitoring (Figure S1) shows that the running catalytic solution absorbs at 482 nm indicating that the catalyst active in

amidine formation is $[1.Fe^V(NTs)]^{2+}$.³¹ We then resorted to computational investigations to obtain mechanistic insights able to explain all experimental observations and consistent with the chemical features of the active species and substrates.

DFT calculations

(i) Methodology.

Our previous DFT investigations of the electronic structure of the active species $[1.Fe^{IV}(NTs)]^{2+}$ and $[1.Fe^V(NTs)]^{2+}$ have highlighted the intrinsic complexity of the electronic structure of open shell Fe binuclear systems bearing radical ligands.^{30,31} Performing reliable calculations of reaction pathways using a hybrid functional as B3LYP, and transition state (TS) searches including frequency calculations is impracticable owing to the size of these complexes. As before, we turned to monoiron models built from $[2.Fe^{II}(NCMe)_2]$ (Scheme 2b) which has shown similar albeit more modest reactivity (see above). In our previous mechanistic studies of aziridination mechanisms,^{33,34} we used the mononuclear model $[2.Fe^{IV}(NTs)]^{37}$ (which is formed by reaction of PhI=NTs with the precursor $[2.Fe^{II}(NCMe)_2]$). In the present work, we considered its one electron oxidized analog $[2.Fe^V(NTs)]^+$ to model the $[1.Fe^V(NTs)]$ active species identified by UV-visible experiments.

In order to get insights into the mechanism of amidine formation, we have envisaged several plausible reaction *scenarii* and tested them using DFT calculations. We started by considering the generation of a second potential active species by acetonitrile binding $[2.Fe^V(NTs)(NCMe)]^+$. We then studied the amination reaction of EB mediated by both active species along the usual hydrogen atom transfer (HAT) and rebound processes.³⁸ Turning to amidination, we examined three pathways, starting either from acetonitrile-free or acetonitrile-bound active species. We also analyzed how changing substrate from EB to cyclohexane affects the thermodynamics of the reactions and this will be presented in the Discussion Section.

(ii) Choice and electronic structure of the model active species; equilibrium of acetonitrile binding.

We have thus explored the $[2.Fe^V(NTs)]^+$ species and its acetonitrile complex $[2.Fe^V(NTs)(NCMe)]^+$. In these species, the Fe^V ion in d³ configuration gives rise to a quartet (S=3/2) and a doublet (S=1/2) state. Our previous calculations of $[2.Fe^{IV}(NTs)]$ showed that the $[2.H_2]$ ligand contributes a small ligand field.^{33,37} When turning to the Fe^V model without or with acetonitrile bound, the calculations of the spin state ordering with various hybrid functionals (TPSSH, B3LYP and PBE0, see Table S1) showed that although the quartet state is the ground state, the doublet state is almost degenerate. This led us to ex-

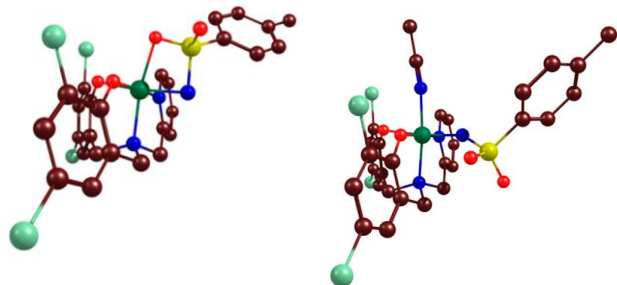
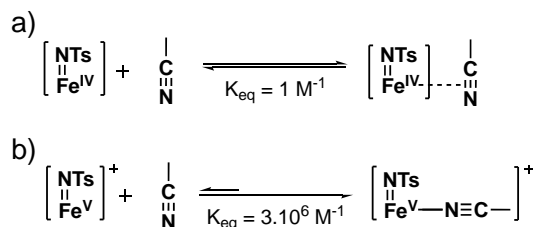


Figure 2. Left: optimized structure of $[2.\text{Fe}^{\text{V}}(\text{NTs})]^+$ model; right: optimized structure of $[2.\text{Fe}^{\text{V}}(\text{NTs})(\text{NCMe})]^+$ model. H atoms not represented, Fe atoms in green, N atoms in blue, O atoms in red and Cl atoms in light green.

explored all reaction pathways on the quartet surface and most of them on the doublet surface. Geometry optimization of the acetonitrile adduct $[2.\text{Fe}^{\text{V}}(\text{NTs})(\text{NCMe})]^+$ shows that NTs binds preferentially in the equatorial plane and acetonitrile axially (Figure 2, right). In absence of acetonitrile, NTs binds the Fe ion in $[2.\text{Fe}^{\text{V}}(\text{NTs})]^+$ with an SO_2 oxygen bound axially (Figure 2, left). The main features of geometry optimizations, spin densities and relative energies of spin states without and with acetonitrile bound to Fe^{V} are summarized in Tables S1 and S2. Examination of the spin densities reveals an electronic configuration consistent with a $[2.\text{Fe}^{\text{IV}}(\cdot\text{NTs})]$ species. Another low-lying excited configuration with a $[2\cdot.\text{Fe}^{\text{IV}}(\text{NTs})]$ and a radical character on the phenolate *cis* to the NTs group is also observed. The same behavior is observed with $[2.\text{Fe}^{\text{V}}(\text{NTs})(\text{NCMe})]^+$. Such behavior is reminiscent of the actual binuclear $[1.\text{Fe}^{\text{V}}(\text{NTs})]^{2+}$ complex which exhibited two tautomers with an Fe^{IV} and a radical either on NTs or on the phenolate ligand.³¹

Scheme 4. Computational studies of acetonitrile binding to a) $[2.\text{Fe}^{\text{IV}}(\text{NTs})]$ and b) $[2.\text{Fe}^{\text{V}}(\text{NTs})]^+$.



Our previous calculations showed that acetonitrile binds $[2.\text{Fe}^{\text{IV}}(\text{NTs})]$ very weakly and in a side-on geometry (Scheme 4a).^{33,37} By contrast acetonitrile binds $[2.\text{Fe}^{\text{V}}(\text{NTs})]^+$ in an end-on geometry through the N atom and the enthalpy of the equilibrium is evaluated by DFT to $-8.8 \text{ kcal mol}^{-1}$ in favor of the acetonitrile complex (Scheme 4b). This difference in acetonitrile binding mode is in agreement with an increase of the acidic character of the complex upon oxidation from Fe^{IV} to Fe^{V} . These first results are consistent with the observation that amidine formation is catalyzed by $[1.\text{Fe}^{\text{V}}(\text{NTs})(\text{NCMe})]^{2+}$ deduced by UV-visible monitoring and the observation of a saturation behavior when acetonitrile concentration is varied. In addition, an electron-rich nitrile should have a higher binding constant thus favoring the nitrile adduct and thereby formation of the amidine, what is observed. In the following paragraphs, we will consider the amination of EB by $[2.\text{Fe}^{\text{V}}(\text{NTs})]^+$ and $[2.\text{Fe}^{\text{V}}(\text{NTs})(\text{NCMe})]^+$, and its amidination either by bulk MeCN or by the acetonitrile-bound active species $[2.\text{Fe}^{\text{V}}(\text{NTs})(\text{NCMe})]^+$.

(iii) *Amination pathways of ethylbenzene by $[2.\text{Fe}^{\text{V}}(\text{NTs})]^+$*

Few amination studies with full computed pathways have been published³⁹⁻⁴² and they all show the so-called stepwise process of HAT followed by a rebound step, that we have thus investigated here. The thermodynamic profile for the amination of ethylbenzene by $[2.\text{Fe}^{\text{V}}(\text{NTs})]^+$ on the quartet surface (Figure

3) starts with the formation of the reactant complex (Re) followed by an HAT process with a very low electronic energy activation ($4.3 \text{ kcal mol}^{-1}$) which yields the expected $\text{Fe}^{\text{IV}}\text{-NHTs}$ species and a methylbenzyl radical (Figure 3, Int1). The TS of the rebound process from Int1 to the product (Pdt) could not be identified. As a matter of fact, this elementary step is controlled by the $\text{C}_\alpha\text{-N}_{(\text{NHTs})}$ distance reaction coordinate which decreases during the rebound process. This process triggers an electron transfer (ET) from the radical substrate to the Fe center owing to an increase in the oxidizing nature of the Fe ion due to NHTs departure. This ET occurs abruptly defining a maximum energy point as appearing on the scan. This point was evaluated by very tight steps along this reaction coordinate. More details on this computation of the rebound energy are given in SI (Computational details section). Analogous difficulties in the rebound process had been already underlined in a few previous articles, either for the imido group^{39,41} or even for the oxo group.⁴³ The details of the molecular structures of the intermediate and product are shown in Figure S3 and Table S3 and S4. The amination profile has also been calculated in the doublet state for $[2.\text{Fe}^{\text{V}}(\text{NTs})]^+$ and the comparison for both spin states is illustrated in Figure S2. It shows that the doublet is not favored with higher energies for activation barriers and intermediates.

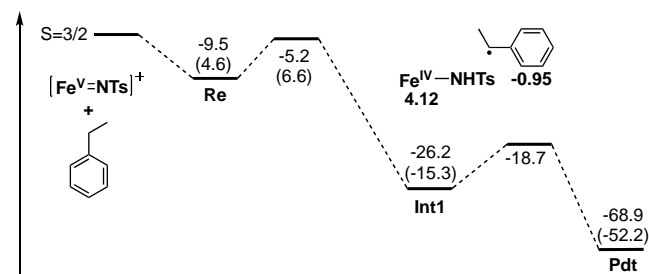


Figure 3. Electronic energies (Gibbs energies in parentheses) in kcal mol^{-1} for the amination of ethylbenzene from $[2.\text{Fe}^{\text{V}}(\text{NTs})]^+$, calculated at the B3LYP-D3/BS2_COSMO//B3LYP-D3/BS1 level. Spin densities on Fe and on methylbenzyl radical in the intermediate Int1 are shown in bold.

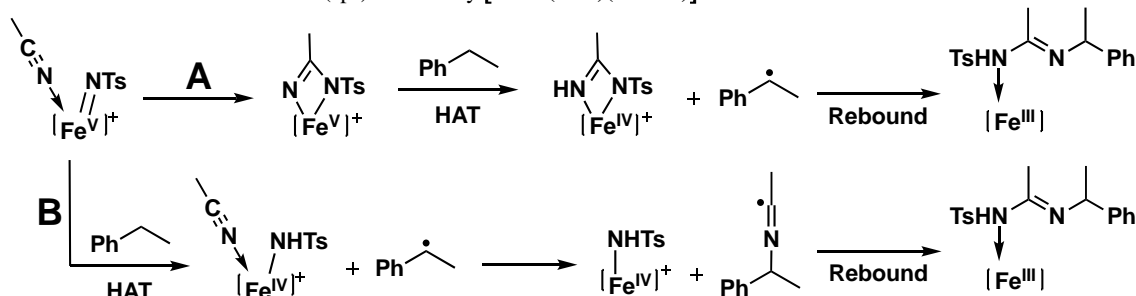
(iv) *Amination pathways of ethylbenzene by $[2.\text{Fe}^{\text{V}}(\text{NTs})(\text{NCMe})]^+$*

From $[2.\text{Fe}^{\text{V}}(\text{NTs})(\text{NCMe})]^+$ (Figure S4 and Table S5), the profile starts again with an HAT process with a low electronic energy activation ($7.6 \text{ kcal mol}^{-1}$) leading similarly to the expected $\text{Fe}^{\text{IV}}\text{-NHTs}$ species and a methylbenzyl radical (Int1, see Figure S5 and Table S6). Again the TS for rebound could not be identified and the electronic energy difference is given instead (see Figure S6). It is worth noting that, as previously, this barrier is the highest one in the reaction. The rebound process occurs again with the electron transfer to the Fe center with a higher activation energy ($21.7 \text{ kcal mol}^{-1}$ on the quartet surface) compared to the previous rebound without acetonitrile coordinated ($7.5 \text{ kcal mol}^{-1}$, see Figure 3). Consistently, the C - N bond formation occurs earlier (i.e. the $\text{N}_{(\text{NHTs})} - \text{C}_\alpha$ distance at the maximum point is longer) for the $[2.\text{Fe}^{\text{V}}(\text{NTs})]^+$ species (i. e. 2.60 \AA) than for the $[2.\text{Fe}^{\text{V}}(\text{NTs})(\text{NCMe})]^+$ species (2.38 \AA). Both of these features are in agreement with an electron transfer and rebound more difficult in the latter case than in the former. Acetonitrile binding also affects the initial HAT with a slight increase of the activation free energy ($5.1 \text{ vs } 2.0 \text{ kcal mol}^{-1}$) consistent with a decrease of the electro-

philic character of the active species. Finally, it should be mentioned that the doublet surface parallels the quartet one with similar activation energies for both spin states (Figure S4). To summarize, our calculations show that binding of

acetonitrile to the Fe^{V} catalyst drastically lowers its ability to perform the amination of ethylbenzene by increasing the energy barrier of the rebound process which is the rate determining step (RDS) in both cases.

Scheme 5. Mechanism for amination of a $\text{C}(\text{sp}^3)\text{-H}$ bond by $[\mathbf{2.Fe}^{\text{V}}(\text{NTs})(\text{NCMe})]^+$.



(v) Amidination pathways of ethylbenzene by $[\mathbf{2.Fe}^{\text{V}}(\text{NTs})(\text{NCMe})]^+$

Acetonitrile insertion can occur at different stages of the reaction depending on its binding to Fe: (i) a Fe-bound acetonitrile can combine with the nitrene to give a new acetamidine-nitrene²⁵ (diazaferracyclobutane) (Scheme 5A), or (ii) it can trap a radical or cation from the substrate within Fe coordination sphere (Scheme 5B), and alternatively (iii) a bulk acetonitrile can trap a substrate radical or cation.²⁶ We have considered these three possibilities successively. It followed that formation of a diazaferracyclobutane is feasible but with a prohibitive thermodynamic cost (23 kcal mol⁻¹) compared to other possible pathways, as detailed in Figure S7, Tables S7 and S8. Similarly, trapping of a substrate radical by an outer-sphere (bulk) acetonitrile before nitrene rebound faces a complicated and thermodynamically costly rebound (see SI and Figure S8).

We were thus led to consider process (ii) in which nitrile insertion occurs in the course of the amination process as shown

in Scheme 5 path B. We started by investigating the energetic profile of pathway B in detail. Figure 4 shows the amidination process of ethylbenzene on the quartet surface and Figure S9 on the doublet surface.

The reaction profile starts with the same HAT as the amination described above in paragraph iv leading to Int1 (Figure 4). Then, an electron transfer step occurs from the methylbenzyl radical to Fe, leading to a methylbenzyl cation and a $\text{Fe}^{\text{III}}\text{-NHTs}$ species with acetonitrile partly de-coordinated (Int2), as revealed by the spin densities and charges. As a matter of fact, the spin density (sd) on the methylbenzyl radical vanishes (sd = 0.96 \rightarrow 0) while a charge develops (q = 0 \rightarrow 0.77) on going from Int1 to Int2. The de-coordination of acetonitrile from Fe is certainly the factor triggering this electron transfer as it renders the Fe^{IV} ion more oxidizing. It is worth noting that the acetonitrile nitrogen is at similar distance from Fe and substrate C_α in Int2. The activation profile associated to this de-coordination coupled to ET process

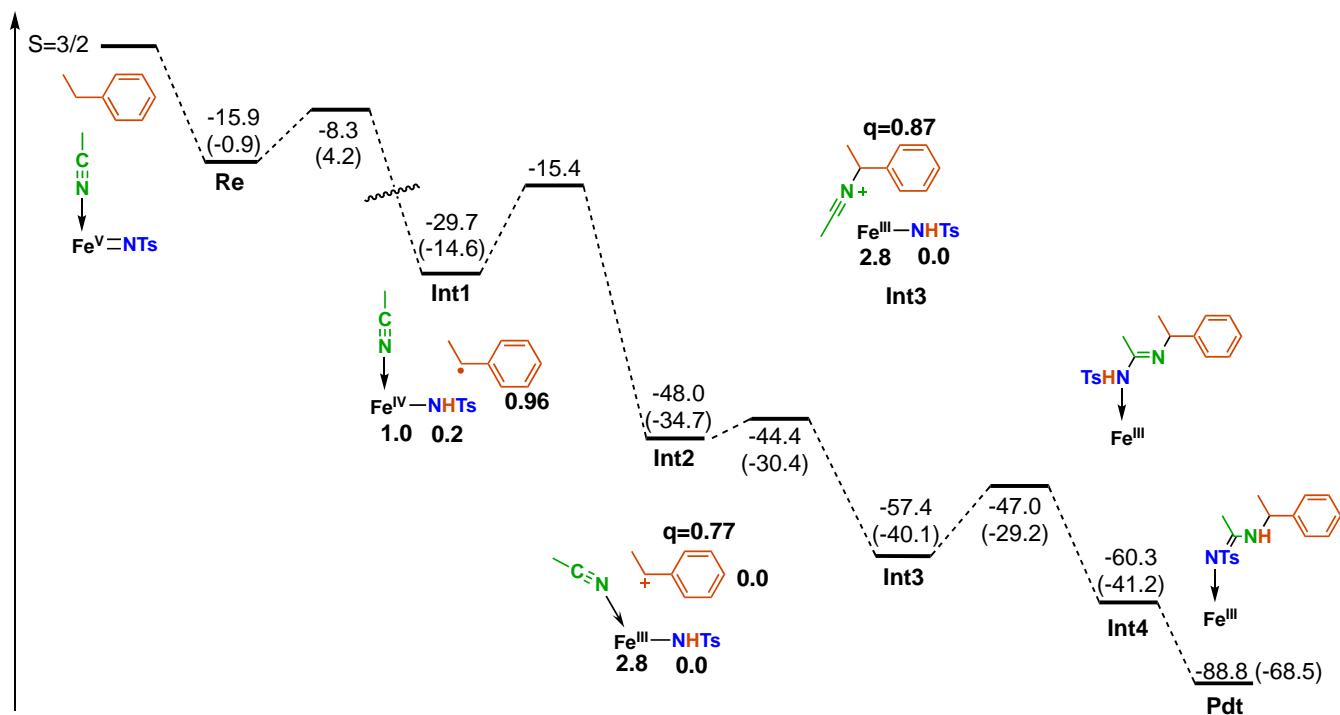


Figure 4. Electronic energies (Gibbs energies in parentheses) in kcal mol⁻¹ for acetonitrile insertion during the amidination of ethylbenzene from the Fe^V active species in quartet state, calculated at the B3LYP-D3/BS2_COSMO//B3LYP-D3/BS1 level. The energy origin corresponds to isolated reactants. Some electronic features of the intermediates Int1-3 are shown (spin densities in bold and Mulliken charge q). Full details are in Figure S9 and Table S10. The kinked orientation of acetonitrile in Int2 is indicative of its partial decoordination.

shows again an abrupt fall which precludes the identification of the TS. Therefore, the electronic activation energy of this step is estimated based on tight scans (see SI and Table S9) to be 14.3 kcal mol⁻¹. Then the bonding of acetonitrile to the methylbenzyl cation occurs to yield Int3 which features an acetiminium cation ($q = 0.87$), with a very low barrier (3–4 kcal mol⁻¹). The next step is the rebound of NHTs to form Int4 with a barrier of *ca* 10 kcal mol⁻¹. Int4 then rearranges to the product (Pdt) through a tautomeric proton exchange. The largest barrier in the whole process (14.3 kcal mol⁻¹) is that of the ET after the initial HAT process. Looking at the doublet surface (Figure S9), we observe a similar behavior with a profile parallel to the quartet one. The molecular structures of the intermediates are shown on Figure S10 and Table S10. To summarize, this mechanism based on an inner-sphere acetonitrile attack of the methylbenzyl radical/cation fully explains amidine formation.

(vi) Summary of mechanistically relevant features

The computational exploration of the various possible reaction pathways for yielding amine and amidine EB derivatives has thus brought several insightful informations. Focusing first on amidine formation, the process involving a metallacycle (amidinate coordinated to Fe ion) is not plausible due to the high activation energy necessary to its formation. Trapping of a benzyl radical by bulk acetonitrile does not appear likely either owing to a disfavored rebound pathway (Figure S8). The active species responsible for amidination is thus proposed to be $[2.\text{Fe}^{\text{V}}(\text{NTs})(\text{NCMe})]^{\dagger}$ in good agreement with i) THF experiments, ii) the existence of a binding equilibrium of acetonitrile and iii) the low activation energy of the reaction (14 kcal mol⁻¹, Figure 4). Interest-

ingly, the calculations rationalized that the facile amine formation from $[2.\text{Fe}^{\text{V}}(\text{NTs})]^{\dagger}$ is under control of nitrile binding which shuts it down and revealed that amidine and amine formation processes from $[2.\text{Fe}^{\text{V}}(\text{NTs})(\text{NCMe})]^{\dagger}$ diverge after H⁺ abstraction, which is consistent with a competitive production of both compounds in a fixed ratio, amidine formation being favored.

Experimental validation of the proposed mechanism

Several mechanistic features have emerged from the above DFT calculations which differ from those suggested by Bagchi *et al.*²⁶ In particular, all molecular events occur exclusively within the coordination sphere of the Fe catalyst or at least in a neighboring cage as opposed to bulk solution reactivity. This prompted us to try and get experimental evidence to support the following points: (i) the N atom bound to the substrate originates from acetonitrile (and not TsNH₂), both (ii) oxidation of the substrate radical and (iii) attack of the resulting acetiminium cation by tosylamine occur in close proximity to Fe ion. We have therefore endeavored to get a validation of the above conclusions through a combination of radical trap experiments with CBrCl₃ and specific labeling experiments using ¹⁵N-labeled tosylamine and CH₃C¹⁵N.

(i) Acetonitrile is the source of the N atom bound to the substrate

As a consequence of acetonitrile attack of the substrate cation, the nitrogen atom bound to the substrate would come from acetonitrile and not from the nitrene. We obtained the X-ray structure of the amidine derived from cyclohexane,

namely *N*-(cyclohexyl)-*N'*-tosylacetimidamide (Figure 5), full details on the structure are given in Figure S11 and Tables S11-S13). It is very similar to that of *N*-(1-phenylethyl)-*N'*-tosylacetimidamide reported by Bagchi *et al.*²⁶ and shows the *E*-*syn* configuration of the amidine function between the substrate and the tosyl group.⁴⁴ However, it does not provide any clue on the origins of the two N atoms. As a matter of fact, the possibility that the substrate-bound nitrogen N2 comes from the tosyliminiodinane cannot be ruled out owing to the fact that tosyl migration has been observed in similar reactions in certain instances.⁴⁵

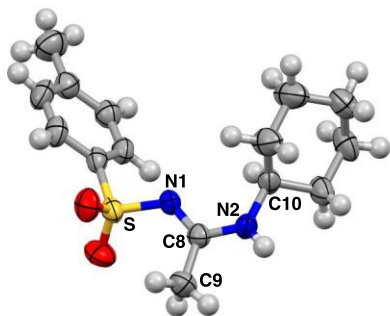


Figure 5. X-ray structure of *N*-cyclohexyl-*N'*-tosylacetimidamide. Selected bond distances (Å) and angles (°): C8-N1 1.318(2), C8-N2 1.323(2), C10-N2 1.452(2), S-N1 1.5953(13), C8-C9 1.493(3), N1-C8-N2 117.53(15), N1-C8-C9 126.22(16), N2-C8-C9 116.25(16), C8-N2-C10 125.34(15), C8-N1-S 122.08(11)

To answer this question beyond any doubt, we performed the catalytic aminations of ethylbenzene using ¹⁵N labeled reagents, Ts¹⁵NH₂ and/or CH₃C¹⁵N, and analyzed the composition of *N*-(1-phenylethyl)-*N'*-tosylacetimidamide and *N*-(1-phenylethyl)-*N*-tosylamine with ESI-MS and ¹⁵N-NMR. In a series of experiments ethylbenzene was treated in a 9/1 mixture of dichloromethane/acetonitrile for 5h at 25 °C in the conditions [1.Fe^{II}(NCMe)]²⁺/PhI(OAc)₂/TsNH₂/ethylbenzene 0.05/1/1/50 and the isotopic composition of TsNH₂ and CH₃CN was varied.

A first experiment was run using PhI(OAc)₂/Ts¹⁵NH₂ in pure dichloromethane (DCM, Figure S12). Analysis of the reaction mixture by ¹⁵N-NMR in CD₃CN showed the presence of a triplet of 1:2:1 intensities at 94 ppm *vs* aqueous NH₃, *J* = 80 Hz indicative of *J*_{15N-1H} coupling) which is the signature of Ts¹⁵NH₂ (Figure 6a). In addition, two doublets were present at 109 and 104 ppm (*J*_{15N-1H} = 88 Hz) that were assigned, respectively, to the amine Ph-CH(Me)-¹⁵NHTs and methylene-bis-tosylamine Ts¹⁵NH-CH₂-¹⁵NHTs, a known side product.²⁶ In addition, a singlet was observed at 245 ppm which corresponds to CD₃C¹⁵N (natural abundance of CD₃CN). Analysis of the crude mixture from a second experiment (Figure S13) run in DCM/CH₃C¹⁵N using PhI(OAc)₂/Ts¹⁵NH₂ showed the presence of three new signals, one singlet at 214 ppm and two doublets at 131 and 138 ppm (*J*_{15N-1H} = 92 Hz) (Figure 6d). Therefore, these must be associated to the amidine.

To assign them further we performed experiments with different labeling of the CH₃CN/TsNH₂ reagents. We started by labeling TsNH₂ (reaction in DCM/CH₃CN using PhI(OAc)₂/Ts¹⁵NH₂, Figure S14) and ¹⁵N-NMR analysis showed only the presence of the 214 ppm singlet (Figure 6b). These observations show that the NTs group in the amidine is not protonated and therefore part of an imine. It can there-

fore be tentatively assigned to the amidine Ph-CH(Me)-NH-(Me)C=¹⁵NTs. This assignment is supported by a recent experimental and theoretical investigation of the ¹⁵N-NMR spectrum of famotidine which has assigned at 216 ppm the signal of a nitrogen in a similar environment RR'-C=N-SO₂-R".⁴⁶

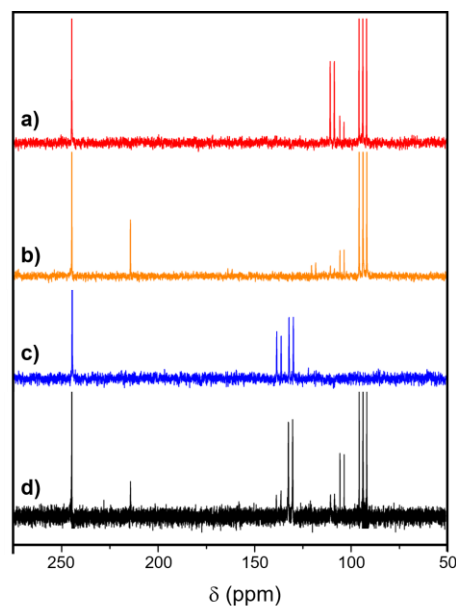


Figure 6. ¹⁵N-NMR spectra in CD₃CN of the reaction mixtures of catalytic amination of ethylbenzene in presence of Ts¹⁵NH₂ or CH₃C¹⁵N: a) Ts¹⁵NH₂ absence of CH₃CN, b) Ts¹⁵NH₂ and CH₃CN, c) CH₃C¹⁵N and TsNH₂, and d) Ts¹⁵NH₂ and CH₃C¹⁵N. (See Figures S12 - S14, S16 for detailed assignments.)

This assignment is also consistent with the ESI-MS fragmentation pattern of the Na⁺ adduct of amidine from this reaction which identified the successive losses of styrene and CH₃CN to yield Ts¹⁵NH₂ as terminal fragment (Figure S15). Quite consistently ¹⁵N-NMR analysis of the reverse experiment (reaction in DCM/CH₃C¹⁵N using PhI=NTs, Figure S16) evidenced only the two doublets at 131 and 138 ppm (Figure 6c) and ESI-MS fragmentation the losses of styrene and CH₃C¹⁵N to the final TsNH₂ fragment (Figure S17). The two remaining doublets at 131 and 138 ppm are thus likely associated to the amidine Ph-CH(Me)-¹⁵NH-C(Me)=NTs group. The amidine Ph-CH(Me)-NH-C(Me)=NTs can indeed exist as two isomers with the tosyl and methyl groups located on the same side (*E* isomer) of the imine double bond or the opposite one (*Z* isomer).⁴⁴ It must be noted that the values of the chemical shifts and the coupling constants of these doublets are close to those of the amine Ph-CH(Me)-¹⁵NHTs (Figure 6a) in agreement with a similar structure. To summarize, these ¹⁵N-NMR experiments indicate that the nitrogen bound to ethylbenzene benzylic carbon originates from acetonitrile as suggested by the DFT study.

(ii) Radical trap experiments

DFT calculations suggest that an intermediate benzylmethyl radical is formed through H[•] abstraction and further oxidized to the corresponding cation before being trapped by acetonitrile released from Fe. If diffusion of the radical occurred and its oxidation done in bulk solution, it would be trapped by a radical scavenger. Raising the scaven-

ger concentration would favor this reaction at the expense of amidine formation. We thus studied the catalytic amination of ethylbenzene in the presence of increasing amounts of CBrCl_3 up to 20 equivalents per mole of catalyst. No effect could be detected on amidine formation, in agreement with a process occurring exclusively in Fe immediate vicinity.

(iii) *Tosylamide rebound occurs within Fe close proximity*

The last issue that we addressed is whether the recombination of the acetiminium cation occurs with Fe-bound or "caged" tosylamide/tosylamine as opposed to in bulk solution with tosylamine. Tosylamine can undoubtedly be released from Fe tosylamide complex by adventitious protonation. To investigate this point we performed a catalytic experiment in usual conditions (catalyst/PhI=NTs/ethylbenzene = 0.05/1/50) but in the presence of 1 equivalent Ts- ^{15}N H $_2$ added at the start of the reaction. The final reaction mixture was analyzed by ^1H -NMR and ESI-MS and both analysis failed to show incorporation of ^{15}N Ts in the amidine, again in agreement with a process occurring exclusively in Fe immediate vicinity.

DISCUSSION

Our combined experimental and theoretical studies have delineated the main mechanistic features, which allows a rationalization of both (i) the formation of amidines through combined nitrene transfer and acetonitrile insertion, and (ii) the distributions of amine and amidine depending on substrate nature and acetonitrile concentration.

Mechanism of amidine formation

In the following paragraphs we will examine the main aspects of this mechanism and contrast them to previous proposals.

(i) The formation of an intermediate diazametallacyclobutane (Metal = Mn, Fe) was initially proposed by Evans *et al.*²⁵ and formation of such a copper species was very recently evidenced by Bakhoda *et al.*²⁷ Such metal species can be viewed as amidinates and are well known in the literature, notably with Fe.⁴⁷⁻⁴⁹ In addition, examples of formation of this kind of species within a metal coordination sphere abound. For Pt complexes they were shown to be intermediates in amidine formation through amide attack of nitriles.^{18,19} The mechanism of the reaction has been studied in depth by Zhang *et al.* for a ruthenium anilide complex and they evidenced the required prior binding of acetonitrile to the Ru anilide followed by intramolecular nucleophilic addition of the anilide.^{50,51} Our calculations show that a diazaferracyclobutane could be formed in the conditions of our catalytic experiments. However, the activation enthalpy associated to its formation by nitrene attack of acetonitrile outweighs by ca $> 15 \text{ kcal mol}^{-1}$ the one associated to H $^\bullet$ abstraction making amidinate formation highly unlikely and inconsistent with our experimental finding that amidine formation is favored over amine formation. It is noteworthy that the formation of a similar azaferracyclobutane as intermediate in aziridine formation was studied by Isbill *et al.* and rejected on the same ground.⁵² This leads to consider that amidine formation should occur through acetonitrile interception of a substrate-derived intermediate, radical or cation.

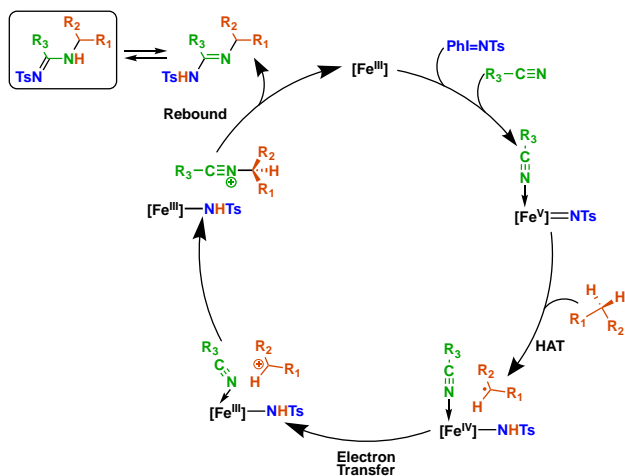
(ii) Bagchi *et al.* proposed that after H $^\bullet$ abstraction by the nitrene, the radical (R $^\bullet$) escapes from the catalyst and gets oxidized to the corresponding cation (R $^+$).²⁶ The latter is then trapped by acetonitrile giving an acetiminium cation (R-N=C(Me) $^+$) which forms the amidine by reaction with bulk tosylamine (R-NH-C(Me)=NTs).²⁶ Our studies using the same radical trap agent CBrCl_3 failed to detect any effect, which shows that the two systems behave differently. Our DFT studies allowed us to clarify the oxidation pathway and showed that the tosyl amide recombines with the substrate within Fe coordination sphere (see below). As a matter of fact, our calculations showed that an electron transfer immediately follows H $^\bullet$ abstraction (Figures 4 and S9): owing to the Fe high-valent state of the active species, the $[\text{Fe}^{\text{IV}}\text{-NHTs}]$ amido species resulting from HAT is powerful enough to oxidize the radical. The coupling of electron transfer with nitrene transfer has recently been noted in several instances in sulfimidation^{38,53} and aziridination^{54,55}, but in only one in amination by Sastri, de Visser and coworkers from their DFT study of benzylic oxidation by the well-known $[(\text{N4Py})\text{Fe}^{\text{IV}}(=\text{NTs})]$ complex.^{38,56} The different behavior of the above copper complex may reside in the fact that the Cu^{II} species resulting from H $^\bullet$ abstraction is not powerful enough to oxidize the radical rapidly, allowing for its escape in solution.

(iii) Another point of interest in this process is the fact that in the Fe^{III} species resulting from combined H $^\bullet$ abstraction and electron transfer, acetonitrile binding is weakened, which may facilitate its attack of the cation. Whereas this attack could occur in bulk solution, our calculations suggest that it takes place within the coordination sphere of the metal. Indeed, as shown by the optimized structure of the corresponding intermediate (Int 2 in Figures 4 and S10) the acetonitrile N is at similar distances (3.1 Å) of the Fe and the benzylic carbon of the substrate.

(iv) The last step towards amidine formation is the binding of the TsNH $^\bullet$ group to the iminium cation. By contrast, our calculations suggest that this process occurs in the coordination sphere of the metal or at least in its immediate vicinity. Our experiments performed in the presence of free ^{15}N -labeled tosylamine failed to show any ^{15}N labeling of amidine, which excludes reaction in bulk solution. This process is thus likely to occur as a rebound, immediately after formation of the benzyl cation in Fe vicinity (see ii above) and may explain the different behavior proposed by Bagchi *et al.*²⁶

All these mechanistic features are incorporated in the following scheme (Scheme 6) that we view as the most plausible major reaction steps in the catalytic cycle.

Scheme 6. Proposed reaction mechanism of Fe-catalyzed amidine formation.

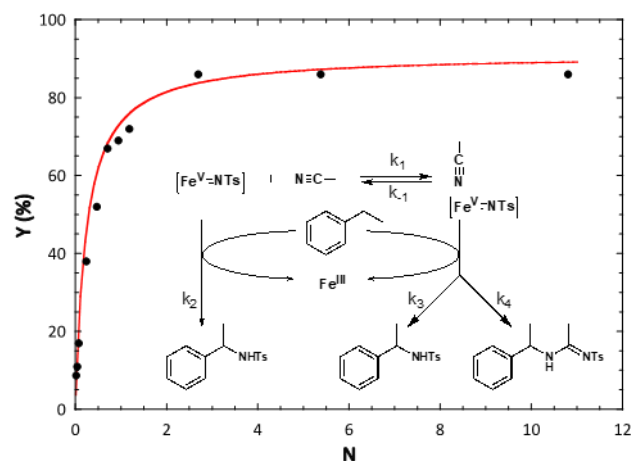


Rationalization of amidine vs amine formation

Coming now to the overall reactivity landscape, our experimental studies have shown that amidine formation is under control of both the concentration of acetonitrile and the BDE of the hydrocarbon substrate. Both features can be rationalized from our DFT analyses.

Focusing first on the transformations of ethylbenzene, the experimental data presented in Figure 1 have revealed that two regimes can be distinguished depending on the acetonitrile / ethylbenzene ratio N . When acetonitrile concentration increases the (amidine / amine + amidine) distribution (Y) increases until N reaches 1.2 after which Y is constant and close to 0.9. The existence of these two regimes can be likely rationalized as follows. In the first regime, the speciation is controlled by MeCN binding equilibrium. As a consequence, initial amine formation catalyzed by $[2.\text{Fe}^{\text{V}}(\text{NTs})]^+$ is progressively outbalanced through its depletion by acetonitrile binding giving $[2.\text{Fe}^{\text{V}}(\text{NTs})(\text{NCMe})]^+$ until $N \approx 1.2$ where this amination route is shut down. At $N > 1.2$, only $[2.\text{Fe}^{\text{V}}(\text{NTs})(\text{NCMe})]^+$ is present. The DFT analyses of amidine and amine formations from $[2.\text{Fe}^{\text{V}}(\text{NTs})(\text{NCMe})]^+$ have shown that H^\bullet abstraction is common to both processes and thus the observed amidine / amine distribution reflects the different efficacies of the two "rebound" processes, with and without acetonitrile insertion. The competitions between these different processes are summarized in Schemes 7.

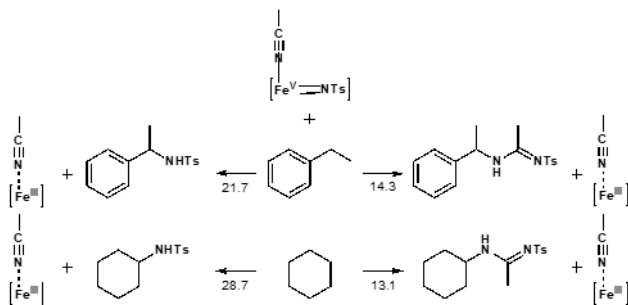
Scheme 7. General mechanism for amine vs amidine formation for ethylbenzene (inset) and kinetic simulation.



To account for all experimental observations, we initially resorted to a thermodynamical model (Figure S18) built according to Michaelis-Menten equation.³⁵ However, whereas this model allowed us to simulate the saturation curve of Figure 1 quite satisfactorily, the value of the equilibrium constant deduced from the fitting ($K = 3.03 \text{ M}^{-1}$) strongly differed from the one estimated by DFT ($K = 3 \cdot 10^6 \text{ M}^{-1}$). This discrepancy prompted us to elaborate a phenomenological kinetic model (Scheme 7 and S1) taking into account the acetonitrile binding equilibrium ($K = k_1/k_{-1}$), the apparent initial amination rate constant (k_2), and the amidination and amination rate constants (k_4 and k_3 , respectively). Albeit this simplified model (see SI) did not allow us to determine all individual constants (Table S14), it could reproduce the data quite satisfactorily (Figure S19 and Scheme 7) and, in all conditions studied, revealed some interesting features: (i) a high acetonitrile binding equilibrium constant K ca 10^7 M^{-1} allows to reproduce the experimental data, what is consistent with the value $\Delta G = -8.8 \text{ kcal mol}^{-1}$ estimated at $T = 0 \text{ K}$ by DFT, (ii) a constant k_1 / k_2 ratio is found close to 4.2, which indicates a faster binding of acetonitrile with respect to amination of EB by $[2.\text{Fe}^{\text{V}}(\text{NTs})]^+$ in line with acetonitrile shutting down amination and consistent with the barrier-less acetonitrile binding from DFT calculations and (iii) a constant k_4 / k_3 ratio is found close to 10 as found on the plateau at $N \geq 1.2$, which expresses a more efficient rebound for amidination over amination, consistent with DFT calculations. The importance of these various competitive processes is illustrated in Figure S20 which represents the variations of amine and amidine produced by the different routes as a function of N .

When cyclohexane replaces ethylbenzene as substrate no amine is formed which is likely due to its higher BDE (99 vs 85 kcal mol^{-1}). To investigate how this change in BDE can affect the reactivity, we computed, using the same DFT approach, the amination and amidination reaction profiles with cyclohexane as detailed in Figures S21 - S24 and Tables S15 - S18. These calculations showed that the activation barrier for amination of cyclohexane by $[2.\text{Fe}^{\text{V}}(\text{NTs})]^+$ is significantly increased with respect to EB (12.5 vs 7.5 kcal mol^{-1} , compare Figures 3 and S21). This ca 5 kcal mol^{-1} increase makes amination uncompetitive with acetonitrile binding. Concerning amine vs amidine formation by $[2.\text{Fe}^{\text{V}}(\text{NTs})(\text{NCMe})]^+$ again the activation energy for amine formation is ca 7 kcal mol^{-1} higher in case of cyclohexane vs ethylbenzene (28.7 vs 21.7 kcal mol^{-1} , compare Figures S4 and S21) whereas it is unchanged for amidine formation (Scheme 8). This explains the exclusive formation of amidine for cyclohexane.

Scheme 8. Summary of the RDS activation energies in the processes of amination (left) or amidination (right) by $[2.\text{Fe}^{\text{V}}(\text{NTs})(\text{NCMe})]^+$, for both substrates: ethylbenzene (top) and cyclohexane (bottom).



CONCLUSION

Understanding the mechanism of catalytic one-pot reactions is notoriously difficult.⁵⁷ However, their special interest in the search for ever greener chemical syntheses has very recently motivated several groups to develop integrated experimental and computational studies aimed at deciphering how they operate. In the present work, the deep interplay between experiments and theory allowed us to delineate the molecular mechanism of amidine synthesis from combined nitrene transfer and nitrile insertion to hydrocarbons and to show that all individual molecular events occur in Fe vicinity. Moreover, the thermodynamics issued from the various reaction profiles were instrumental to rationalize the amine vs amidine competitive formations over the full range of acetonitrile vs substrate ratio. In practical terms, this offers a way to access a large variety of amidines in good yields and under mild conditions. This work thus highlights the strength of these kinds of approaches.^{5,57–59}

ASSOCIATED CONTENT

Supporting Information

The Supporting Information is available free of charge at <https://pubs.acs.org/doi/>.

X-ray structure of *N*-cyclohexyl-*N'*-tosylacetamidine CHTosMe (CIF)

Experimental details; synthesis procedures; characterizations; ¹⁵NMR, ESI-MS

Computational details; reaction profiles and relaxed scans; molecular and thermodynamic properties as well as Cartesian coordinates of stationary points

Thermodynamic and kinetic modeling of the experimental data

AUTHOR INFORMATION

Corresponding Authors

Pascale Maldivi – Univ. Grenoble Alpes, CEA, CNRS, IRIG, DIESE, SYMMES, 38000 Grenoble, France; Email: pascale.maldivi@cea.fr

Jean-Marc Latour – Univ. Grenoble Alpes, CEA, CNRS, IRIG, DIESE, LCBM, 38000 Grenoble, France; orcid.org/0000-0002-9939-4542; Email: jean-marc.latour@cea.fr

Author Contributions

The manuscript was written through contributions of all authors. All authors have given approval to the final version of the manuscript.

Notes

The authors declare no competing financial interest.

ACKNOWLEDGMENTS

J.-M. L. and P. M. thank the Labex ARCANE and CBH-EUR-GS (ANR-17-EURE-0003) for partial funding. This work was performed using HPC resources from GENCI (Grants A0020807648, A0040807648 and A0060807648). Mr J. Batbedat is thanked for experimental assistance.

REFERENCES

- (1) Hayashi, Y. Pot Economy and One-Pot Synthesis. *Chem. Sci.* **2016**, *7*, 866–880.
- (2) Wan, J.-P.; Gan, L.; Liu, Y. Transition Metal-Catalyzed C–H Bond Functionalization in Multicomponent Reactions: A Tool toward Molecular Diversity. *Org. Biomol. Chem.* **2017**, *15*, 9031–9043.
- (3) Ahn, S.; Hong, M.; Sundararajan, M.; Ess, D. H.; Baik, M.-H. Design and Optimization of Catalysts Based on Mechanistic Insights Derived from Quantum Chemical Reaction Modeling. *Chem. Rev.* **2019**, *119*, 6509–6560.
- (4) Kruihof, A.; Mulder, J. R.; Ruiz, J. M.; Janssen, E.; Mooijman, M.; Ruijter, E.; Guerra, C. F.; Bickelhaupt, F. M.; Orru, R. V. A. Integrative Theory/Experiment-Driven Exploration of a Multicomponent Reaction towards Imidazoline-2-(Thi)Ones. *Eur. J. Org. Chem.* **2018**, 104–112.
- (5) van Vliet, K. M.; Polak, L. H.; Siegler, M. A.; van der Vlugt, J. I.; Guerra, C. F.; de Bruin, B. Efficient Copper-Catalyzed Multicomponent Synthesis of *N*-Acyl Amidines via Acyl Nitrenes. *J. Am. Chem. Soc.* **2019**, *141*, 15240–15249.
- (6) Xie, S.; Manuguri, S.; Proietti, G.; Romson, J.; Fu, Y.; Inge, A. K.; Wu, B.; Zhang, Y.; Hall, D.; Ramstrom, O.; Yan, M. Design and Synthesis of Theranostic Antibiotic Nanodrugs That Display Enhanced Antibacterial Activity and Luminescence. *Proc. Natl. Acad. Sci. U. S. A.* **2017**, *114*, 8464–8469.
- (7) Lv, Z.; Wang, B.; Hu, Z.; Zhou, Y.; Yu, W.; Chang, J. Synthesis of Quinazolines from *N,N'*-Disubstituted Amidines via I-2/KI-Mediated Oxidative C-C Bond Formation. *J. Org. Chem.* **2016**, *81*, 9924–9930.
- (8) Cao, V. D.; Mun, S. H.; Kim, S. H.; Kim, G. U.; Kim, H. G.; Joung, S. Synthesis of Cyclic Amidines from Quinolines by a Borane-Catalyzed Dearomatization Strategy. *Org. Lett.* **2020**, *22*, 515–519.
- (9) Houck, J. D.; Dawson, T. K.; Kennedy, A. J.; Kharel, Y.; Naimon, N. D.; Field, S. D.; Lynch, K. R.; Macdonald, T. L. Structural Requirements and Docking Analysis of Amidine-Based Sphingosine Kinase 1 Inhibitors Containing Oxadiazoles. *ACS Med. Chem. Lett.* **2016**, *7*, 487–492.
- (10) Jamali, H.; Khan, H. A.; Tjin, C. C.; Ellman, J. A. Cellular Activity of New Small Molecule Protein Arginine Deiminase 3 (PAD3) Inhibitors. *ACS Med. Chem. Lett.* **2016**, *7*, 847–851.
- (11) Bae, I.; Han, H.; Chang, S. Highly Efficient One-Pot Synthesis of *N*-Sulfonylamidines by Cu-Catalyzed Three-Component Coupling of Sulfonyl Azide, Alkyne, and Amine. *J. Am. Chem. Soc.* **2005**, *127*, 2038–2039.
- (12) Kim, J.; Stahl, S. S. Cu-Catalyzed Aerobic Oxidative Three-Component Coupling Route to *N*-Sulfonyl Amidines via an Ynamine Intermediate. *J. Org. Chem.* **2015**, *80*, 2448–2454.
- (13) Kim, M. J.; Kim, B. R.; Lee, C. Y.; Kim, J. *N*-Sulfonyl Amidine Synthesis via Three-Component Coupling Reaction Using Heterogeneous Copper Catalyst Derived from Metal-Organic Frameworks. *Tetrahedron Lett.* **2016**, *57*, 4070–4073.
- (14) Zhang, Z.; Huang, B.; Qiao, G.; Zhu, L.; Xiao, F.; Chen, F.; Fu, B.; Zhang, Z. Tandem Coupling of Azide with Isonitrile and

- Boronic Acid: Facile Access to Functionalized Amidines. *Angew. Chem.-Int. Ed.* **2017**, *56*, 4320–4323.
- (15) Xu, X.; Gao, H.; Cheng, D.; Li, J.; Qiang, G.; Guo, H. Copper-Catalyzed Highly Efficient Multicomponent Reactions of Terminal Alkynes, Acid Chloride, and Carbodiimides: Synthesis of Functionalized Propiolamide Derivatives. *Adv. Synth. Catal.* **2008**, *350*, 61–64.
- (16) dos Santos, M. S.; Rolim Bernardino, A. M.; de Souza, M. C. Synthetic Approaches to Amidines. *Quimica Nova* **2006**, *29*, 1301–1306.
- (17) Harjani, J. R.; Liang, C.; Jessop, P. G. A Synthesis of Acetamidines. *J. Org. Chem.* **2011**, *76*, 1683–1691.
- (18) Kukushkin, V. Y.; Pombeiro, A. J. L. Additions to Metal-Activated Organonitriles. *Chem. Rev.* **2002**, *102*, 1771–1802.
- (19) Michelin, R. A.; Mozzon, M.; Bertani, R. Reactions of Transition Metal-Coordinated Nitriles. *Coord. Chem. Rev.* **1996**, *299*–338.
- (20) Saluste, C. G.; Whitby, R. J.; Furber, M. A Palladium-Catalyzed Synthesis of Amidines from Aryl Halides. *Angew. Chem. Int. Ed.* **2000**, *39*, 4156–4158.
- (21) Kim, S. H.; Jung, D. Y.; Chang, S. Phosphoryl Azides as Versatile New Reaction Partners in the Cu-Catalyzed Three-Component Couplings. *J. Org. Chem.* **2007**, *72*, 9769–9771.
- (22) Dai, Q.; Jiang, Y.; Yu, J.-T.; Cheng, J. Palladium-Catalyzed Three-Component Reaction of N-Tosyl Hydrazones, Isonitriles and Amines Leading to Amidines. *Chem. Commun.* **2015**, *51*, 16645–16647.
- (23) Zhang, Y.; Chen, Z. Three Component Reaction of Aryl Diazonium Salt with Sulfonamide & Acetonitrile to Synthesize N-Sulfonyl Amidine. *Tetrahedron Lett.* **2018**, *59*, 4183–4186.
- (24) Liu, B.; Ning, Y.; Virelli, M.; Zanoni, G.; Anderson, E. A.; Bi, X. Direct Transformation of Terminal Alkynes into Amidines by a Silver-Catalyzed Four-Component Reaction. *J. Am. Chem. Soc.* **2019**, *141*, 1593–1598.
- (25) Evans, D. A.; Faul, M. M.; Bilodeau, M. T. Development of the Copper-Catalyzed Olefin Aziridination Reaction. *J. Am. Chem. Soc.* **1994**, *116*, 2742–2753.
- (26) Bagchi, V.; Paraskevopoulou, P.; Das, P.; Chi, L.; Wang, Q.; Choudhury, A.; Mathieson, J. S.; Cronin, L.; Pardue, D. B.; Cundari, T. R.; Mitrikas, G.; Sanakis, Y.; Stavropoulos, P. A Versatile Tripodal Cu(I) Reagent for C–N Bond Construction via Nitrene-Transfer Chemistry: Catalytic Perspectives and Mechanistic Insights on C–H Aminations/Amidinations and Olefin Aziridinations. *J. Am. Chem. Soc.* **2014**, *136*, 11362–11381.
- (27) Bakhoda, A.; Jiang, Q.; Bertke, J.; Cundari, T. R.; Warren, T. H. Elusive Terminal Copper Aryl Nitrene Intermediates. *Angew. Chem. Int. Ed.* **2017**, *56*, 6426–6430.
- (28) Chardon-Noblat, S.; Horner, O.; Chabut, B.; Avenier, F.; Debaecker, N.; Jones, P.; Pécaut, J.; Dubois, L.; Jeandey, C.; Oddou, J.-L.; Deronzier, A.; Latour, J.-M. Spectroscopic and Electrochemical Characterizations of an Aqua Ligand Exchange and Oxidatively-Induced Deprotonation in Diiron Complexes. *Inorg. Chem.* **2004**, *43*, 1638–1648.
- (29) Avenier, F.; Gouré, E.; Dubourdeaux, P.; Sénèque, O.; Oddou, J.-L.; Pécaut, J.; Chardon-Noblat, S.; Deronzier, A.; Latour, J.-M. Multiple Aromatic Amination Mediated by a Diiron Complex. *Angew. Chem. Int. Ed.* **2008**, *47*, 715–717.
- (30) Gouré, E.; Avenier, F.; Dubourdeaux, P.; Sénèque, O.; Albrieux, F.; Lebrun, C.; Clémancey, M.; Maldivi, P.; Latour, J.-M. A Diiron(III,IV) Imido Species Very Active in Nitrene-Transfer Reactions. *Angew. Chem. Int. Ed.* **2014**, *53*, 1580–1584.
- (31) Gouré, E.; Senthilnathan, D.; Coin, G.; Albrieux, F.; Avenier, F.; Dubourdeaux, P.; Lebrun, C.; Maldivi, P.; Latour, J.-M. Redox Self-Adaptation of a Nitrene Transfer Catalyst to the Substrate Needs. *Angew. Chem. Int. Ed.* **2017**, *56*, 4305–4309.
- (32) Avenier, F.; Latour, J.-M. Catalytic Aziridination of Olefins and Thioether Amidation by a Non-Heme Iron Complex. *Chem. Commun.* **2004**, 1544–1545.
- (33) Patra, R.; Coin, G.; Castro, L.; Dubourdeaux, P.; Clémancey, M.; Pécaut, J.; Lebrun, C.; Maldivi, P.; Latour, J.-M. Rational Design of Fe Catalysts for Olefin Aziridination through DFT-Based Mechanistic Analysis. *Catal. Sci. Technol.* **2017**, *7*, 4388–4400.
- (34) Coin, G.; Patra, R.; Clémancey, M.; Dubourdeaux, P.; Pécaut, J.; Lebrun, C.; Castro, L.; Maldivi, P.; Chardon-Noblat, S.; Latour, J.-M. Fe-Based Complexes as Styrene Aziridination Catalysts: Ligand Substitution Tunes Catalyst Activity. *ChemCatChem* **2019**, *11*, 5296–5299.
- (35) Johnson, K. A.; Goody, R. S. The Original Michaelis Constant: Translation of the 1913 Michaelis–Menten Paper. *Biochemistry* **2012**, *51*, 8264–8269.
- (36) Luo, Y.-R. *Handbook of Bond Dissociation Energies in Organic Compounds*; Chapter 3. Tabulated BDEs of C–H bonds. CRC Press: Boca Raton, 2002.
- (37) Patra, R.; Maldivi, P. DFT Analysis of the Electronic Structure of Fe(IV) Species Active in Nitrene Transfer Catalysis: Influence of the Coordination Sphere. *J. Mol. Model.* **2016**, *22*, 278.
- (38) Kumar, S.; Faponle, A. S.; Barman, P.; Vardhaman, A. K.; Sastri, C. V.; Kumar, D.; de Visser, S. P. Long-Range Electron Transfer Triggers Mechanistic Differences between Iron(IV)-Oxo and Iron(IV)-Imido Oxidants. *J. Am. Chem. Soc.* **2014**, *136*, 17102–17115.
- (39) Moreau, Y.; Chen, H.; Derat, E.; Hirao, H.; Bolm, C.; Shaik, S. NR Transfer Reactivity of Azo-Compound I of P450. How Does the Nitrogen Substituent Tune the Reactivity of the Species toward CH and CC Activation? *J. Phys. Chem. B* **2007**, *111*, 10288–10299.
- (40) Li, Z.; Burnell, D. J.; Boyd, R. J. Computational Study of Engineered Cytochrome P450-Catalyzed C–H Amination: The Origin of the Regio- and Stereoselectivity. *J. Phys. Chem. B* **2017**, *121*, 10859–10868.
- (41) Li, X.; Dong, L.; Liu, Y. Theoretical Study of Iron Porphyrin Nitrene: Formation Mechanism, Electronic Nature, and Intermolecular C–H Amination. *Inorg. Chem.* **2020**, *59*, 1622–1632.
- (42) Wang, J.; Gao, H.; Yang, L.; Gao, Y. Q. Role of Engineered Iron-Haem Enzyme in Reactivity and Stereoselectivity of Intermolecular Benzylic C–H Bond Amination. *ACS Catal.* **2020**, *10*, 5318–5327.
- (43) Singh, R.; Ganguly, G.; Malinkin, S. O.; Demeshko, S.; Meyer, F.; Nordlander, E.; Paine, T. K. A Mononuclear Nonheme Iron(IV)-Oxo Complex of a Substituted N4Py Ligand: Effect of Ligand Field on Oxygen Atom Transfer and C–H Bond Cleavage Reactivity. *Inorg. Chem.* **2019**, *58*, 1862–1876.
- (44) Kalz, K. F.; Hausmann, A.; Dechert, S.; Meyer, S.; John, M.; Meyer, F. Solution Chemistry of N,N'-Disubstituted Amidines: Identification of Isomers and Evidence for Linear Dimer Formation. *Chem. Eur. J.* **2016**, *22*, 18190–18196.
- (45) Bendlkov, M.; Duong, H. M.; Bolanos, E.; Wudl, F. An Unexpected Two-Group Migration Involving a Sulfonylamide to Nitrile Rearrangement. Mechanistic Studies of a Thermal N f C Tosyl Rearrangement. *Org. Lett.* **2005**, *7*, 783–786.
- (46) Marosi, A.; Szalay, Z.; Béni, S.; Szakacs, Z.; Gati, T.; Racz, A.; Noszal, B.; Demeter, A. Solution-State NMR Spectroscopy of Famotidine Revisited: Spectral Assignment, Protonation Sites, and Their Structural Consequences. *Anal. Bioanal. Chem.* **2012**, *402*, 1653–1666.
- (47) Barker, J.; Kilner, M. The Coordination Chemistry of the Amidine Ligand. *Coord. Chem. Rev.* **1994**, *133*, 219–300.
- (48) Rose, R. P.; Jones, C.; Schulten, C.; Aldridge, S.; Stasch, A. Synthesis and Characterization of Amidinate-Iron(I) Complexes: Analogies with Beta-Diketiminato Chemistry. *Chem.-Eur. J.* **2008**, *14*, 8477–8480.
- (49) Yu, Y.; Sadique, A. R.; Smith, J. M.; Dugan, T. R.; Cowley, R. E.; Brennessel, W. W.; Flaschenriem, C. J.; Bill, E.; Cundari, T. R.; Holland, P. L. The Reactivity Patterns of Low-Coordinate Iron-Hydride Complexes. *J. Am. Chem. Soc.* **2008**, *130*, 6624–6638.
- (50) Zhang, J.; Gunnoe, T. B.; Boyle, P. D. Ruthenium(II) Anilido Complex Containing a Bisphosphine Pincer Ligand: Reversible Formation of Amidinate Ligands via Intramolecular C–N Bond Formation. *Organometallics* **2004**, *23*, 3094–3097.
- (51) Zhang, J.; Gunnoe, T. B.; Petersen, J. L. Reactions of (PCP)Ru(CO)(NHPh)(PMe₃) (PCP) 2,6-(CH₂PtBu₂)₂C₆H₃ with

Substrates That Possess Polar Bonds. *Inorg. Chem.* **2005**, *44*, 2895–2907.

(52) Isbill, S. B.; Chandrachud, P. P.; Kern, J. L.; Jenkins, D. M.; Roy, S. Elucidation of the Reaction Mechanism of C2 + N1 Aziridination from Tetracarbene Iron Catalysts. *ACS Catal.* **2019**, *9*, 6223–6233.

(53) van Leest, N. P.; van der Vlugt, J. I.; de Bruin, B. Catalytic Chemoselective Sulfimidation with an Electrophilic [CoIII(TAML)]--Nitrene Radical Complex. *Chem Eur J* **2020**, Accepted article.

(54) Coin, G.; Patra, R.; Rana, S.; Biswas, J. P.; Dubourdeaux, P.; Clemancey, M.; de Visser, S. P.; Maiti, D.; Maldivi, P.; Latour, J.-M. Fe-Catalyzed Aziridination Is Governed by the Electron Affinity of the Active Imido-Iron Species. *ACS Catal.* **2020**, *10*, 10010–10020.

(55) van Leest, N. P.; Tepaske, M. A.; Venderbosch, B.; Oudsen, J.-P. H.; Tromp, M.; van der Vlugt, J. I.; de Bruin, B. Electronically Asynchronous Transition States for C-N Bond Formation by Electrophilic [Co-III(TAML)]-Nitrene Radical Complexes Involving Substrate-to-Ligand Single-Electron Transfer and a Cobalt-Centered Spin Shuttle. *ACS Catal.* **2020**, *10*, 7449–7463.

(56) Vardhaman, A. K.; Barman, P.; Kumar, S.; Sastri, C. V.; Kumar, D.; de Visser, S. P. Comparison of the Reactivity of Nonheme Iron(IV)-Oxo versus Iron(IV)-Imido Complexes: Which Is the Better Oxidant? *Angew. Chem. Int. Ed.* **2013**, *52*, 12288–12292.

(57) Vogiatzis, K. D.; Polynski, M. V.; Kirkland, J. K.; Townsend, J.; Hashemi, A.; Liu, C.; Pidko, E. A. Computational Approach to Molecular Catalysis by 3d Transition Metals: Challenges and Opportunities. *Chem. Rev.* **2019**, *119*, 2453–2523.

(58) Suh, S.-E.; Chen, S.; Houk, K. N.; Chenoweth, D. M. The Mechanism of the Triple Aryne-Tetrazine Reaction Cascade: Theory and Experiment. *Chem. Sci.* **2018**, *9*, 7688–7693.

(59) Wang, X.-G.; Li, Y.; Liu, H.-C.; Zhang, B.-S.; Gou, X.-Y.; Wang, Q.; Ma, J.-W.; Liang, Y.-M. Three-Component Ruthenium-Catalyzed Direct Meta-Selective C-H Activation of Arenes: A New Approach to the Alkylarylation of Alkenes. *J. Am. Chem. Soc.* **2019**, *141*, 13914–13922.

TABLE OF CONTENTS GRAPHICS

